Thermodynamics and fragility of Fe-based glass forming melts

Thermodynamics and fragility of Fe-based glass forming melts

Giulia Dalla Fontana, Alberto Castellero, Livio Battezzati*

Dipartimento di Chimica, Università di Torino, Via Pietro Giuria 7. 10125 Torino, Italy
*corresponding author: livio.battezzati@unito.it

Abstract

Methods to determine the fragility index, *m*, both in thermodynamic and kinetic terms are reviewed and applied to two Fe-based glass formers, $Fe_{40}Ni_{40}P_{14}B_6$ and $Fe_{41}Co_7Cr_{15}Mo_{14}C_{15}B_6Y_2$. The thermodynamic fragility is obtained from entropy curves based on experimental data of the liquid specific heat and of the enthalpy of transformation from glass or liquid to crystal phases.
The thermodynamic fragility appears systematically higher than the kinetic one because of the large scatter of data and their extrapolation to obtain the Kauzmann temperature of vanishing entropy.
A practical method to estimate the viscosity of glass formers in the undercooling regime was derived from the fragility index and its correlation with parameters the VFT equation. It provides reasonable agreement with experimental data.

Keywords

Metallic glasses; Fe amorphous alloys; Thermodynamic properties; Melt fragility; Alloy viscosity

1. Introduction

A liquid supercooled below the melting point (or the liquidus temperature for complex melts) freezes into the glassy state because its viscosity, η, varies of several orders of magnitude until a solid is formed. Conventionally, the value of $\eta = 10^{12}$ Pa·s marks the transition to a glass [1]. The best glass formers have high viscosity already at the melting point, T_m, and the glass transition is reached at temperatures in excess of $0.6 \cdot T_m$, whereas other substances have relatively low viscosity at T_m and the glass transition, T_g, occurs at temperatures of the order of $0.5 \cdot T_m$ [2-3]. The varied trend of viscosity expresses either the strength or fragility of the liquid. The fragility in kinetic terms is defined as the rate of change of a liquid property at the glass transition temperature. According to the Angell's definition [4], the fragility index, m_K, is

$$m_K = \left[\frac{d \log \eta}{d \frac{T_g}{T}} \right]_{T=T_g} \qquad (1)$$

The viscosity of a strong liquid increases with decreasing temperature according to an Arrhenius behaviour, whereas the viscosity of a fragile liquid presents super-Arrhenius behaviour in the range from T_m to T_g [5]. Therefore, high values of m_K indicate a steep rise in viscosity (fragile melt), whereas low values imply steady increase of viscosity with temperature (strong melt). In the potential energy landscape model (PEL) of the liquid various local minima can be accessed by

means of activated processes. For a strong liquid a few deep minima predominate with respect to less deep potential wells whereas the landscape of fragile liquids has several minima of comparable depth. Relaxation times, and therefore viscosity, differ according to the probability of accessing wells of different depth in the specific energy landscape [1].
Extensive thermodynamic quantities vary on undercooling according to landscape configurations: fragile liquids loose entropy faster than strong ones when approaching the glass transition [6]. The amount of entropy frozen in at T_g depends on the trend of the specific heat of the liquid as a function of undercooling. A thermodynamic fragility parameter [7], m_T, is defined as:

$$m_T = \left[\frac{d\frac{\Delta S_g}{\Delta S}}{d\frac{T_g}{T}} \right]_{T=T_g} = \frac{\Delta C_{p,g}}{\Delta S_g} \qquad (2)$$

where ΔS_g and $\Delta C_{p,g}$ are the entropy and the specific heat capacity of the liquid at T_g with respect to a reference state usually taken as the equilibrium crystal [2].
The correlation between kinetic fragility, as expressed by the viscosity behaviour, and thermodynamic fragility, as given by the entropy loss on undercooling, has been discussed in detail within the (PEL) model by expressing the number of local energy minima which can be accessed by melt configurations by means of an energy distribution function and deriving from it the configurational entropy of the liquid at the transition to the glassy state. Assuming the validity of the Adam-Gibbs equation for viscosity [8]: for a Gaussian energy distribution, m is obtained as

$$m_K = 17\frac{T_g^2 + T_K^2}{T_g^2 - T_K^2} \qquad (3)$$

where T_K is the temperature where the entropy difference between the liquid and the equilibrium crystal would vanish (Kauzmann temperature) and 17 are the decades of viscosity values spanned from T_g (10^{12} Pa·s) to the conventional high-temperature limit of 10^{-5} Pa·s. For a hyperbolic energy distribution m_K becomes (first order expansion of eq. (3))

$$m_K = 17\frac{T_g}{T_g - T_K} \qquad (4)$$

Note that the latter position implies that the Adam-Gibbs equation reduces to the Vogel-Fulcher-Tammann (VFT) expression:

$$\eta = A\exp\left[\frac{C}{TS_c}\right] \cong A\exp\left[\frac{B}{T - T_0}\right] \qquad (5)$$

with S_c the configurational entropy of the glass, A, C, B, and T_0 are empirical parameters. T_0 has been assumed equal to T_K. It is also shown that $m_K = 17(m_T+1)$ [8].
Eqs. (3) and (4) suggest a correlation of m derived from experimental viscosity measurements versus T_g/T_K. The values for metallic, inorganic and organic glasses are actually fitted by both equations. Using eq. (5) a distinction between strong (e.g. silicates), intermediate (metallic glasses), and fragile (organic substances) was made. Among metallic glasses, the stronger behaviour is found in La- and Mg- based alloys [9].
No detailed analysis of the fragility of Fe-based glass-formers has been performed to date. This is a major group of metallic glasses used for magnetic applications and also most promising for structural uses in bulk form (e. g. coatings) in view of their extremely high strength and hardness.

Proper knowledge of viscosity and thermodynamics of the undercooled melt would certainly help in designing their processing both for synthesis by melt quenching and for shaping by embossing above T_g [10].

2. Empirical methods to determine *m* and the parameters in the VFT equation for viscosity

The glass transition is most often studied by Differential Scanning Calorimetry (DSC) experiments in which it is marked by a step in the calorimetric curve (with proper calibration the step corresponds to a specific heat difference between undercooled liquid and glass, ΔC_p) occurring in a temperature range from $T_{g,\,onset}$ to $T_{g,\,end}$ (ΔT_g). The extension of this range scaled with respect to T_g is proportional to fragility according to Mohynian's empirical observation that the viscosity change between $T_{g,\,onset}$ and $T_{g,\,end}$ is about two orders of magnitude at conventional heating rates (e.g. 10-40 K/min) [11]. Using the VFT equation, the reduced width of the glass transition provides a value of m_K [12]:

$$\frac{T_{g,\,flex}}{\Delta T_g} \cong \frac{m_K}{2} \qquad (6)$$

where $T_{g,\,flex}$ is the temperature of the inflexion point of the C_p step.
Eq. (1 **)** together with the VFT expression for viscosity implies

$$m_K = BT_g / \left[2.3(T_g - T_0)^2\right] \qquad (7)$$

A correlation between T_0 and B parameters was shown by Wang and Fecht [13] by taking the pre-exponential factor of viscosity as 10^{-5} Pa·s and the viscosity at T_g as 10^{12} Pa·s. The B and T_0 are then related by

$$ln10^{17} = B/(T_g - T_0) \qquad (8)$$

The A parameter in the VFT equation, i. e. the high temperature limit of viscosity, can be obtained from the theory of rate processes as hN_A/V_m, with h and N_A the Planck and Avogadro constants and V_m the molar volume [14]. From the above equations, it turns out that a single adjustable parameter suffices to get a VFT equation.
With the hyperbolic model for the number of states in the PEL it is obtained [8]

$$\frac{\Delta S_g}{\Delta C_{p,g}} = \frac{T_g - T_K}{T_K} = \frac{1}{m_T - 1} \qquad (9)$$

Should ΔS_g, $\Delta C_{p,g}$ and T_g be known from independent experiments or calculations, T_K could be estimated. Following the same procedure with a Gaussian distribution of the states in the PEL, it is obtained

$$\frac{\Delta S_g}{\Delta C_{p,g}} = \frac{T_g^2 - T_K^2}{T_K^2} \qquad (10)$$

In summary the parameters in the VFT equation can be derived, as follows:

- the fragility parameter *m* is obtained from the glass transition span in DSC;
- T_K is obtained from eqs. (3 **)** or (4 **)** and posed equal to T_0;
- eq. (8 **)** provides B.

Alternatively. the *B* and T_0 parameters can be refined by using eq. **Errore. L'origine riferimento non è stata trovata.** and taking the viscosity at the calorimetric onset of T_g at the heating rate of 20 K/min as 10^{11} Pa·s, as found in some experiments [12].

As an alternative route to obtain *m* the empirical formula of Wang and Angell [7] can be used which has proved rather accurate for various inorganic and organic substances

$$m = 56\frac{T_g \Delta C_{p,g}}{\Delta H_m} \qquad (11)$$

where 56 is an empirical parameter, ΔC_p is the specific heat step at T_g and ΔH_m is the enthalpy of melting. We applied eq. **(** 11 **)** to metallic glasses finding that the *m* values generally agree with those derived from viscosity although with larger scatter than for other substances [9, 15].

3. Thermodynamic and viscosity data available for Fe-based amorphous alloys

It is known that Fe-based amorphous alloys exhibit very high strength and hardness which suggest application as coatings [16]. In this respect it is of interest to develop bulk metallic glasses (BMG) having low critical cooling rate for glass formation, comparable to that typical of spray coating processes. The first synthesis of a Fe-based BMG, Fe-Al-Ga-P-C-B, was performed in 1995 [17]; after that several others have been synthesized and characterized. Following up the experience in producing glassy ribbons, the most common elements added to the Fe-alloy are Co and Ni, but other elements such as Ga, Mo, Nb, Zr, Mn, Cr, Al and rare-earths (Y, Er, Gd, Tm) are used to improve the properties and the glass-forming ability [18-29]. A comprehensive overview of the current status of research in Fe-based BMGs has recently appeared [10].

Despite the large quantity of information available on Fe amorphous alloys, there are very few data on the kinetic fragility [30] and the specific heat capacity of these liquids [31]. The data on the specific heat of a solid and an undercooled liquid are expressed respectively by:

$$C_p^s = 3R + aT + bT^2 \qquad (12)$$

$$C_p^l = 3R + cT + dT^{-2} \qquad (13)$$

where *R* is the gas constant, *a*, *b*, *c* and *d* are fitting parameters. Fe-based metallic glasses do not show large supercooled liquid region above T_g, consequently, eq. (**13)** can hardly be used for fitting. Therefore, we have taken the approach of measuring the crystallization, melting and solidification enthalpies at various temperatures to obtain information on thermodynamic properties.

The amorphous $Fe_{40}Ni_{40}P_{14}B_6$ has been obtained both as a BMG and in ribbon form and has been studied extensively for its crystallization behaviour [3, 32-37]. The availability of experimental data on the glass transition temperature (T_g) and crystallization provides means to represent the variation of specific heat versus temperature. Data for the viscosity of $Fe_{40}Ni_{40}P_{14}B_6$ near the glass transition [38-39] and above the liquidus temperature [38] are also available in the literature and can be interpolated with the VFT function [31].

In this work we employ $Fe_{40}Ni_{40}P_{14}B_6$ to check the procedure for determining fragility (both kinetic and thermodynamic) and viscosity described above, and extend it to describe the properties of a liquid of an amorphous steel, $Fe_{41}Co_7Cr_{15}Mo_{14}C_{15}B_6Y_2$, for which much less data are available.

4. Experimental details

The $Fe_{40}Ni_{40}P_{14}B_6$ alloy was prepared in ribbon form (5 mm wide and 8.3 μm thick) by melt spinning using a master alloy prepared by arc melting pure elements and a Fe-P ferro-alloy. Bulk glassy plates of $Fe_{41}Co_7Cr_{15}Mo_{14}C_{15}B_6Y_2$ have been obtained by using copper mold casting.
A high temperature differential scanning calorimetry Setaram HT-DSC was employed to determine thermophysical properties of alloys. The samples were contained in an alumina pan with some Al_2O_3 powder to prevent sticking to the crucible walls. The liquid/solid transformation was followed by high temperature DSC (HT-DSC) by making several melting and solidification cycles of the alloy at different scanning rates.
For $Fe_{40}Ni_{40}P_{14}B_6$, the crystallization has been studied combining the results obtained by DSC and drop calorimetry (DC, Setaram drop head). DSC scans were performed at different rates (Perkin-Elmer DSC7). Isothermal measurements were performed both by DC and DSC. The width of the glass transition range was determined by heating at 30 K/min samples previously relaxed through the same range at the same heating and cooling rate.
Drop calorimetry is suited to obtain the heat content of substances between two temperatures. In this work, the sample at room temperature is dropped into the calorimetric cell kept at constant temperature. When the sample reaches the cell it is heated at high rate. In our experiments the time elapsed in the heating up stage is of the order of 15-20 s implying that the average heating rates to reach temperatures between 668 K and 728 K were in excess of 20 K/s, i. e. 1200 K/min. With high scanning rate the crystallization is displaced to higher temperature in the supercooled liquid region. The procedure was repeated for each sample twice using the amorphous ribbon in the first run and the same crystallized ribbon in the second one [31]. Subtracting the signals obtained in the two runs the heat of crystallization at the temperature of isothermal anneal was derived by integration.

5. Results and Discussion

A DSC scan at 10 K/min gave $T_{g,onset}$ (664 K), $T_{g,end}$ (685 K), and the crystallization temperature, T_x (690 K), of $Fe_{40}Ni_{40}P_{14}B_6$ (Fig. 1). The crystallization occurs very close to the glass transition so the liquid state is not reached in a sufficiently wide range to measure the specific heat in the undercooled liquid. It is reckoned that the glass transition has been completed because the specific heat step was not affected by changing the heating rate from 10 to 100 K/min. Integrating the area of the peak the crystallization enthalpy is obtained, ΔH_x = 5.4 ± 0.3 kJ/mol. The ΔC_p at the glass transition temperature is estimated to be 15.5 ± 2.3 J/molK.

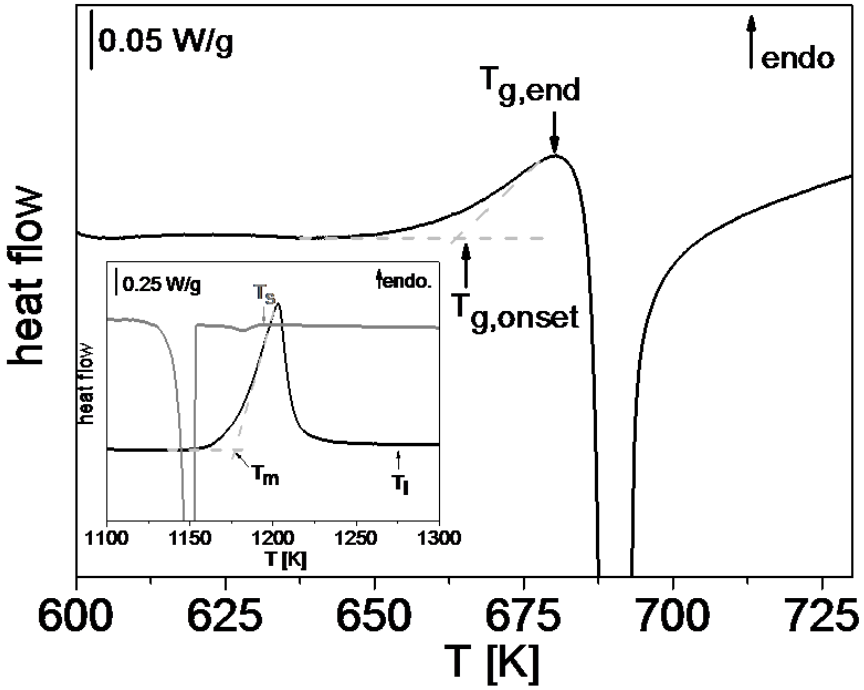

Fig. 1 DSC thermogram of an amorphous $Fe_{40}Ni_{40}P_{14}B_6$ ribbon (heating rate of 10 K/min). The inset reports a HT-DSC scan at 10 K/min of the melting (black line) and solidification (grey line) for the same alloy.

The melting and solidification curves obtained by HT-DSC are shown in the inset of Fig. 1. The eutectic temperature is 1177 ± 2 K, close to the one measured by Miura and Isa [40]. The liquidus temperature, T_l, is 1250 ± 6 K. The single melting peak indicates a eutectic transformation. The melting enthalpy, ΔH_m and the melting entropy, ΔS_m result respectively 11.8 ± 0.3 kJ/mol and 10.0 ± 0.4 J/mol K. Thermal data are collected in
Table **1**. Isothermal measurements by drop calorimetry were performed earlier and in this work were re-analyzed with a revised procedure for overlapping and subtracting the baseline from the first curve [31].
To obtain a reliable expression of the liquid specific heat for $Fe_{40}Ni_{40}P_{14}B_6$ it was devised to use the data on enthalpy.
Fig. **2** contains isothermal crystallization enthalpies obtained by DSC at low temperatures and by drop calorimetry from $T_{g,end}$ (685 K) to 738 K [31], and the melting and solidification enthalpies obtained at high temperature in scanning mode. Furthermore the data of isothermal crystallization enthalpy of bulk samples from DSC as reported by Shen and Schwarz are
reported [3]. The variation in enthalpy depends on the specific heat according to

$$\Delta H^{l-x}(T) = \Delta H_m + \int_{T_{liq}}^{T} \Delta C_p^{l-x}(T')dT' \qquad (14)$$

where *l-x* stands for the differences in property between liquid and crystalline phases.
Employing different expressions for ΔC_p it has been sought to reproduce the trend of the high and low temperature enthalpy data. Simple functions for ΔC_p vs temperature were chosen: T^{-1} to

comply with the VFT equation, T^{-2}, and linear. Moreover, eqs. (12) and (13) suggest a three

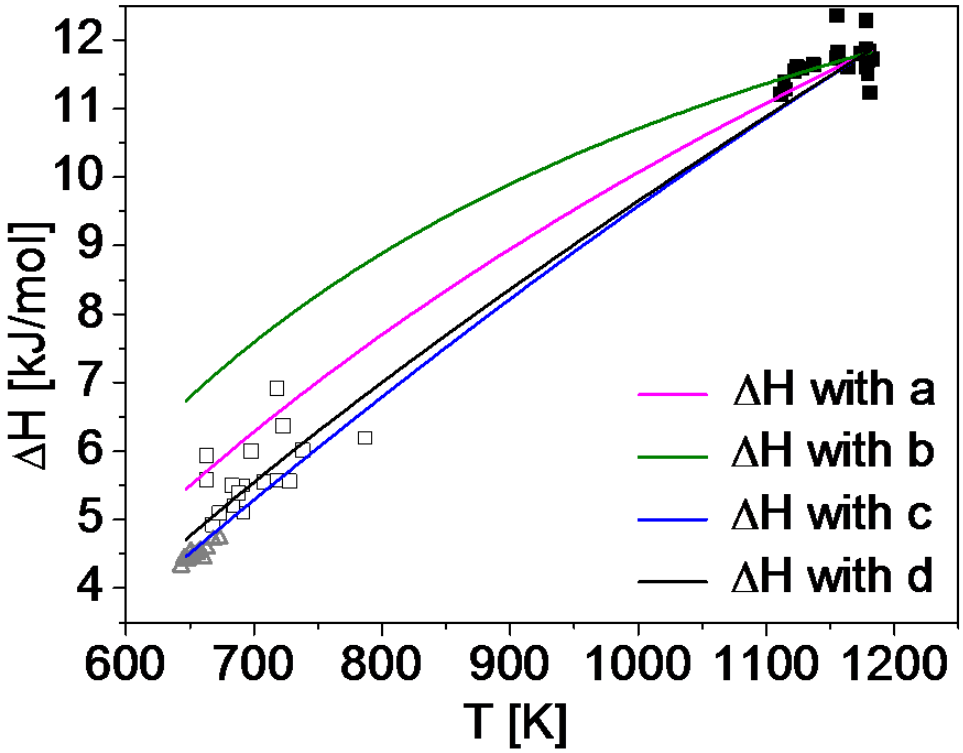

Fig. 2 Experimental crystallization enthalpies obtained by isothermal measurements in drop calorimetry □ [31] and in DSC ▲ [3], and melting-solidification enthalpies obtained in HT-DSC ■[31]. Interpolated curves were computed with different functions for ΔC_p (T): *a* is with $\Delta C_p=A/T$, *b* is with $\Delta C_p=B/T^2$, *c* is with $\Delta C_p=C+D*T$, *d* is with $\Delta C_p=E*T-F*T^2+G*T^{-2}$.

parameters equation, $ET-FT^2+GT^{-2}$. Because of the grouping of the points in two temperature ranges, an unphysical trend of ΔC_p of negative curvature is obtained by simply fitting with it the data points in Fig. 3. To obtain the expected curve for metallic glass-formers, i. e. ΔC_p decreasing with increasing temperature [2,3], we fixed then the values of ΔC_p (T_g), ΔC_p (T_l) and ΔH_x (5.4 J/mol K at the temperature of 690 K). For the functions containing only one parameter (A/T and B/T^2) we fixed $T_{g,end}$ = 685 K and the value of ΔC_p (T_g) at 15.5 J/mol K. For the C+DT linear trend we also imposed the measured value of ΔC_p (T_l) at 11 J/mol K. In this way the parameters *A*, *B*, *C*, *D*, *F* and *G* (see Table A.1 in Supporting information) were obtained for the different trends of ΔC_p.

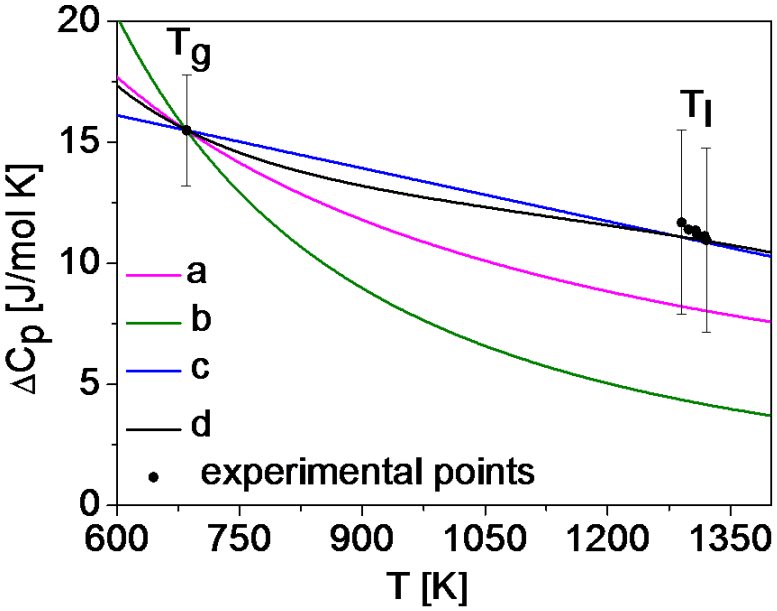

Fig. 3 Comparison of different models (linear, T^{-2} and hyperbolic) to calculate ΔC_p between the liquid and the crystal of $Fe_{40}Ni_{40}P_{14}B_6$. The black circles are experimental points. The value of ΔC_p at T_g is fixed at 15.5 J/mol K. As in Fig. 2 *a* is with $\Delta C_p=A/T$, *b* is with $\Delta C_p=B/T^2$, *c* is with $\Delta C_p=C+D*T$, *d* is with $\Delta C_p=E*T-F*T^2+G*T^{-2}$.

Table 1: Thermal properties of $Fe_{40}Ni_{40}P_{14}B_6$, $Fe_{41}Co_7Cr_{15}Mo_{14}C_{15}B_6Y_2$ alloys.

	T [K]			**ΔH [kJ/mol], ΔS [J/mol K]**	
	$Fe_{40}Ni_{40}P_{14}B_6$	$Fe_{41}Co_7Cr_{15}Mo_{14}C_{15}B_6Y_2$		$Fe_{40}Ni_{40}P_{14}B_6$	$Fe_{41}Co_7Cr_{15}Mo_{14}C_{15}B_6Y_2$
$T_{g,onset}$	664 ± 3	852 ± 3	ΔH_x	5.4 ± 0.3	9.31 ± 0.3
$T_{g\ end}$	685 ± 3	896 ± 3	ΔH_m	11.8 ± 0.3	13.2 ± 0.5
$T_{g\ flex}$	672 ± 3	877 ± 3	ΔS_m	10.0 ± 0.4	12.9 ± 0.3
T_m	1177 ± 2	1420 ± 4		**ΔC_p [J/mol K]**	
T_l	1275 ± 6	1658 ± 4	$\Delta C_p(T_g)$	15.5 ± 2.3	13 ± 2
T_s	1194 ± 2	1369 ± 3	$\Delta C_p(T_l)$	11 ± 3.8	-
T_0	516 ± 30 [31]	-			

The enthalpy functions derived with the above procedure fit generally well the enthalpy data points (
Fig. **2**) with the exception of the T^{-2} one. The specific heat data are obviously well fitted by the two and three parameters equations (Fig. 3) based on fixed values of ΔC_p. It is noted that also the hyperbolic trend reproduces the experimental points within their scatter. The consistency of data has been positively verified according to Eq. (14 **)**.
The entropy loss was computed from the ΔC_p functions, except T^{-2}, according to

$$\Delta S^{\,l-x}(\mathrm{T}) = \Delta S_m + \int_{T_{liq}}^{T} \frac{\Delta C_p^{\,l-x}(T')}{T'} dT' \qquad (15)$$

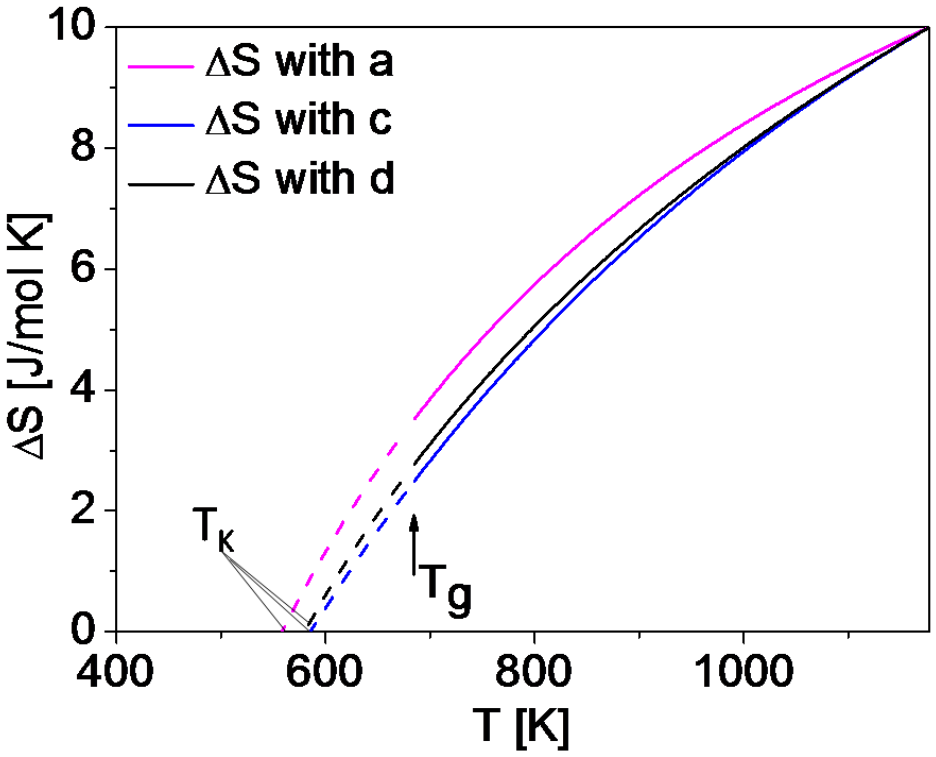

Fig. 4 The entropy difference between undercooled melt and crystal phases of $Fe_{40}Ni_{40}P_{14}B_6$ computed with ΔC_p functions listed for FIG. 2.

The resulting trends of ΔS are shown in Fig. 4 with indication of the Kauzmann temperatures obtained by extrapolation to $\Delta S = 0$ (Table A.1 in Supporting information where error ranges for all quantities are reported). All values of T_K are considerably higher than the T_0 of 516 ± 21 K obtained by fitting viscosity data with the VFT equation [38] although some values remain within the scatter due to cumulative error in the measured quantities. As a consequence of T_K values, the kinetic fragility computed with eqs. (3 **)** and (4 **)**, is higher than that calculated from viscosity (m_K = 69 [31]) (Table A.1 in Supporting information). This was already noted for other metallic glass-formers and attributed to the simplified functions needed to express the parameters and to the experimental uncertainty including the assumption of the crystal as the reference state [9]. Fig. 5 reports the correlation between m_K and the T_g/T_K ratio showing that the metallic glasses generally conform to the behaviour of other glass formers and are located in the lower part of the plot being classified as fragile/intermediate melts [9].

The use of T_K have been recently questioned on the ground that the equality of the entropy of the glass and the crystal is physically impossible [41]. It is underlined that the Kauzmann temperature here is considered as a parameter expressing a hypothetical reference state without attaching to it the physical meaning of a state attainable in experiments. Also, a three parameter expression for viscosity stemming from the Adam-Gibbs model:

$$\log\eta = \log\eta_\infty + \frac{B}{T}\exp\left(\frac{C}{T}\right) \qquad (16)$$

where η_∞ is the viscosity in the high temperature limit and B and C are constants related to the onset of rigidity in the liquid network, was proposed at variance to VFT [42]. The latter resulted from a series expansion of the exponential contained in the new formula. We have checked the two

equation in the temperature range from T_m and T_g for the alloy considered in this work verifying that the viscosity values they provide remain within the scatter of the experimental data. Because of the relationship between the Adam-Gibbs model and the VFT equation leading to eq. (4 **)**, for the sake of simplicity we did not exploit further the new viscosity equation.

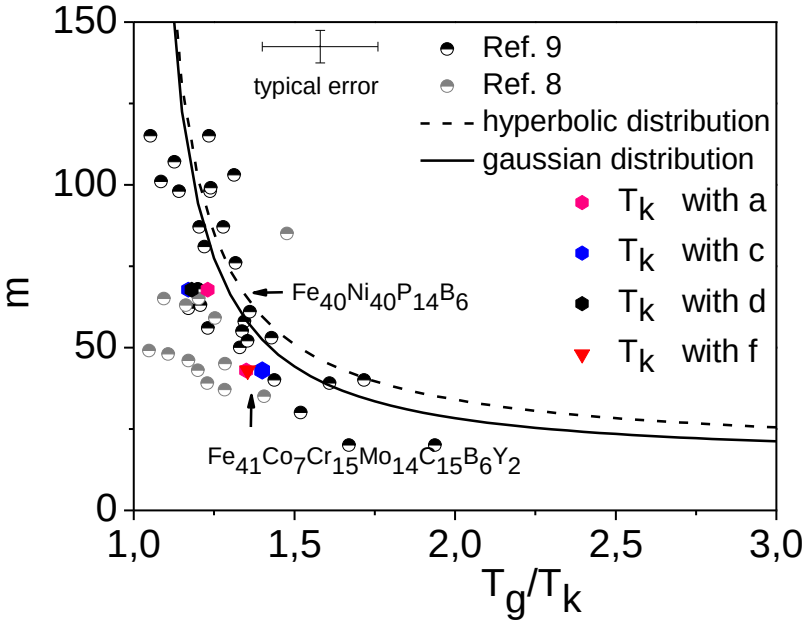

Fig. 5 The kinetic fragility parameter m obtained from viscosity vs the T_g /T_K ratio for metallic and non-metallic glass formers [9]. Those for $Fe_{40}Ni_{40}P_{14}B_6$ and $Fe_{41}Co_7Cr_{15}Mo_{14}C_{15}B_6Y_2$ are highlighted in colour. The full and dashed curves refer to the correlations expressed by Eqs. (3) and (4).

Using the values of quantities listed in Table 1 in eq. (**11)** which does not contain T_K, we obtain m_K = 50 ± 17 again within the scatter of previous data. The best agreement to the value of kinetic fragility derived from viscosity data is obtained using eq. (**6)**: m = 64 ± 18.

With the same procedure employed for $Fe_{40}Ni_{40}P_{14}B_6$ we have computed enthalpies, entropies and fragilities of $Fe_{41}Co_7Cr_{15}Mo_{14}C_{15}B_6Y_2$. This alloy was chosen because its kinetic fragility is reported in the literature, m_K = 43, as derived from viscosity measurements near T_g [30]. This alloy does not show large supercooled liquid region before crystallization, so again we hypothesized different ΔC_p trends in order to fit experimental data on the enthalpies of crystallization, melting and solidification choosing the following functions for ΔC_p: a) $\Delta Cp=A/T$, b) $\Delta Cp=B/T^2$, e) $\Delta Cp=C+D*T$, f) $\Delta Cp=E+F/T$. For a) and b) needing a single parameter we fixed $T_{g,end}$ = 896 K and the value of ΔC_p (T_g) at 13 J/mol K. For e) and f) needing two parameters we also imposed the heat of crystallization and of solidification. For the same reason as for $Fe_{40}Ni_{40}P_{14}B_6$ a three parameter expression cannot be derived. In the case of $Fe_{41}Co_7Cr_{15}Mo_{14}C_{15}B_6Y_2$ all trends of ΔC_p, including the one given by the T^{-2} function, reproduce reasonably the experimental enthalpies (Fig. 6). Furthermore, we can notice that all the values of T_K resulting from the extrapolation of ΔS are very close, see inset of Fig. 6 and Table A.2 in supporting information.

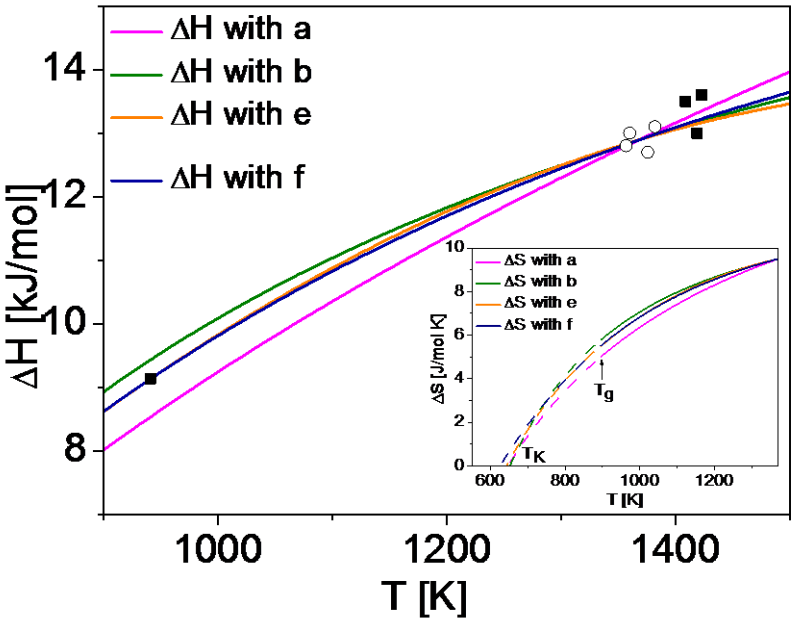

Fig. 6 Experimental crystallization enthalpies and melting-solidification enthalpies obtained in HT-DSC interpolated with different $\Delta C_p(T)$ functions: *a* is with $\Delta C_p=A/T$, *b* is with $\Delta C_p=B/T^2$, *c* is with $\Delta C_p=C+D*T$, *d* is with $\Delta C_p=E+F/T$. The inset shows ΔS trends with extrapolation to nil value at T_K using the different functions for ΔC_p.

The fragilities calculated using eqs. (3) (Gaussian PEL) and (4) (hyperbolic PEL) as well as that obtained by means of eq. (2), are comprised between 49 and 61, somewhat higher than m_K from viscosity [30]. Instead using Angell's formula, eq. (11), we obtained $m_T = 49 \pm 17$ and with eq. (6) m_K is equal to 40 ± 11: both values are close to the kinetic one. Finally, it is noted the scatter both in T_K and m_k are definitely lower for $Fe_{41}Co_7Cr_{15}Mo_{14}C_{15}B_6Y_2$ than for $Fe_{40}Ni_{40}P_{14}B_6$ in spite of having less data available and similar quality of data. This is due to the higher relative value of T_g with respect to T_m and the consequent reduced range of data interpolation.

With the method described in paragraph 2 in which the only quantity linked to viscosity is T_g, we calculated T_0 from eq. (4) and the parameter B from eq. (7 **)** or (8 **)** to obtain a function for viscosity according to VFT eq. (5 **)**. This approximates well the viscosity provided by fitting experimental data [30]. Fig. 7 shows the viscosity of $Fe_{40}Ni_{40}P_{14}B_6$ and $Fe_{41}Co_7Cr_{15}Mo_{14}C_{15}B_6Y_2$ in comparison with a selection of other metallic glass-forming melts and two extreme cases: SiO_2 and o-terphenyl [43]. The SiO_2 is the strongest glass former which shows an Arrhenius variation of the viscosity, instead the o-terphenyl is the most fragile showing pronounced super-Arrhenius behaviour [6]. From Fig. 7 we deduce that $Zr_{44}Ti_{11}Cu_{10}Ni_{10}Be_{25}$ has a stronger character among metallic glass formers and the Fe-alloys are more fragile and similar to some Pt- based glasses [44].

It is stressed, finally, that the present approach provides a practical mean to estimate the viscosity of glass formers in the undercooling regime. This will not be possible in case of the occurrence of a fragile-to-strong transition in this temperature range which might occur in some melts [45]. Its failure, however, can indicate the likelihood of such transition suggesting systems in which it could be revealed.

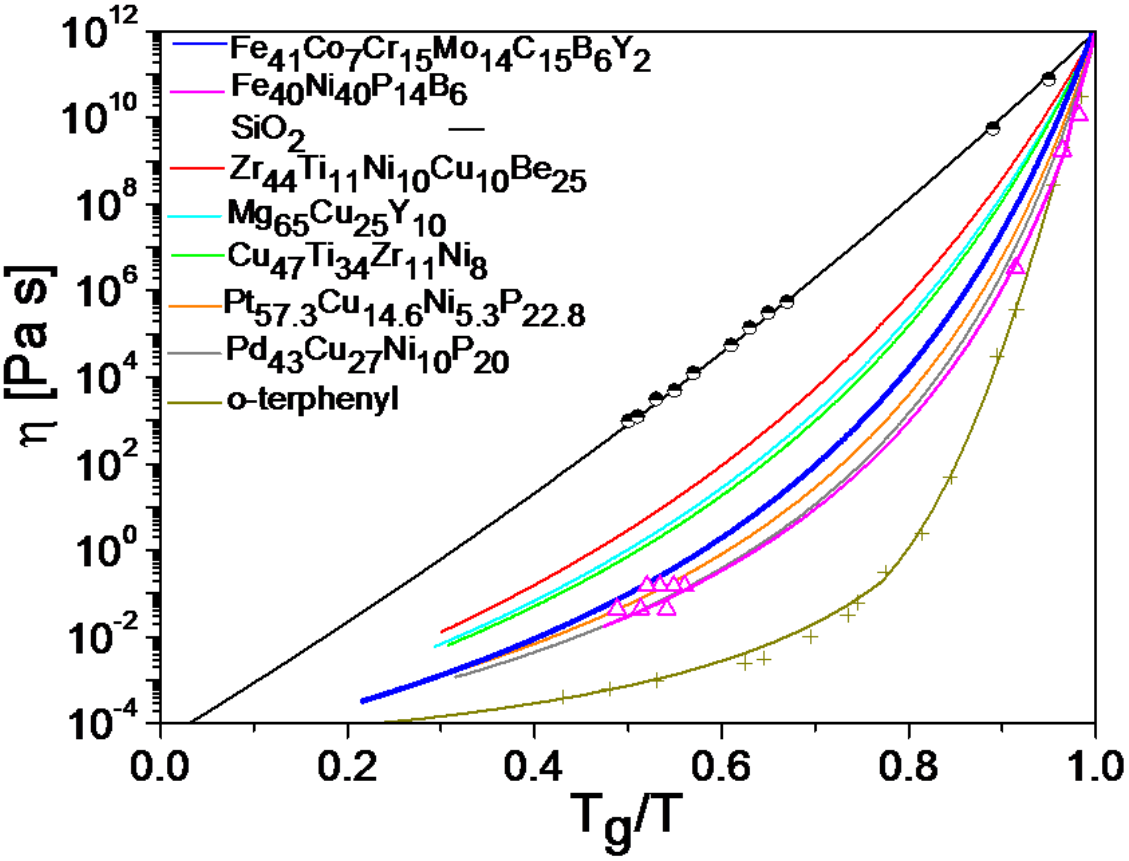

Fig. 7 Angell's plot showing the computed viscosity of Fe-alloys and of other substances and alloys [43] as a function of temperature scaled with respect to T_g i. e. the temperature at which the supercooled liquid viscosity assumes a value of 10^{12} Pa s. Experimental data of viscosity in $Fe_{40}Ni_{40}P_{14}B_6$ at high [39] and low [38] temperatures are given by open triangles. The viscosity curve for $Fe_{40}Ni_{40}P_{14}B_6$ computed with the parameters obtained by applying the procedure outlined in the text falls within the order of magnitude of scatter of experimental data.

Conclusions

In this work the thermodynamics of two Fe-based glass formers, $Fe_{40}Ni_{40}P_{14}B_6$ and $Fe_{41}Co_7Cr_{15}Mo_{14}C_{15}B_6Y_2$ has been reported with the aim of finding a thermodynamic fragility index to be compared with the kinetic ones derived from viscosity and empirical approaches. The supercooled liquid region of both alloys is limited, therefore specific heat capacity data could be measured only at T_g, therefore, the thermodynamic properties were obtained from the enthalpy differences between glass/liquid and crystal phases in temperature ranges just above T_g and around T_m. The enthalpy functions were chosen according to different models for ΔC_p. The experimental data are reproduced by using a one parameter hyperbolic function and two parameters linear and hyperbolic functions. The resulting entropy loss on undercooling provided the thermodynamic fragility m_T computed according to the Gaussian and hyperbolic models of the PEL of the liquid [8]. The m_k was evaluated also using the Angell empirical formula [7]. They differ with respect to the kinetic m_k obtained from viscosity as for other metallic glasses [9] probably because of the large scatter of data and their extrapolation. Instead, there is a good correlation between m_k values obtained from viscosity and the temperature span of the glass transition region.

The fragility values of $Fe_{41}Co_7Cr_{15}Mo_{14}C_{15}B_6Y_2$ are closer to each other than those of $Fe_{40}Ni_{40}P_{14}B_6$ in spite of the lower amount of experimental data possibly because the undercooling range from T_m to T_g is relatively less in the case of the former alloy.
A practical method to estimate the viscosity of glass formers in the undercooling regime has been derived from the fragility index and its correlation with parameters the VFT equation and has been shown to give reasonable agreement with experimental data.

Acknowledgement

This work was supported over the time by the ThermoProp ESA-MAP Project under contract n. 4200014306 (AO -99-022 and AO-2009-1020), by the Italian Space Agency (ASI) under contract n. DC-MIC-2011-036, and by the EU-7FP Accelerated Metallurgy Project (ACCMET, contract NMP4-LA-2011-263206).

References

[1] P.G. Debenedetti, F.H. Stillinger, Nature, 410 (2001) 259-267.
[2] R. Busch, J. Miner. Met. Mater. Soc., 52 (2000) 39-42.
[3] T.D. Shen, R.B. Schwarz, Acta Mater., 49 (2001) 837-847.
[4] R. Bohmer, K.L. Ngai, C.A. Angell, D.J. Plazek, J. Chem. Phys., 99 (1993) 4201-4209.
[5] C.A. Angell, J. Phys. Chem. Solids 49 (1988) 863-871.
[6] L.M. Martinez, C.A. Angell, Nature, 410 (2001) 663-667.
[7] L.M. Wang, C.S. Angell, R. Richert, J. Chem. Phys., 125 (2006) 074505.
[8] G. Ruocco, F. Sciortino, F. Zamponi, C. De Michele, T. Scopigno, J. Chem. Phys., 120 (2004) 10666-10680.
[9] G. Dalla Fontana, L. Battezzati, Acta Mater. , 61 (2013) 2260-2267.
[10] C. Suryanarayana, A. Inoue, Int. Mater. Rev., 58 (2013) 131-166.
[11] C.T. Moyhnian, J. Am. Ceram. Soc., 76 (1993) 1081-1087.
[12] G. Fiore, I. Ichim, L. Battezzati, J. Non-Cryst. Solids, 356 (2010) 2218-2222.
[13] G.J. Fan, R.K. Wunderlich, H.J. Fecht, MRS Symposia Proceedings, 754 (2002) CC5.9.
[14] S.V. Nemilov, Phys. Chem. Glass., 21 (1995) 379-391.
[15] L. Battezzati, G. Dalla Fontana, Journal of Alloys and Compounds, 586 (2014) S9–S13.
[16] X.Q. Liu, Y.G. Zheng, X.C. Chang, W.L. Hou, J.Q. Wang, Z. Tang, A. Burgess, J. Alloys Compd. , 484 (2009) 300-307.
[17] A. Inoue, J.S. Gook, Mater. T. JIM, 36 (1995) 1180-1183.
[18] B. Shen, M. Akiba, A. Inoue, Phys. Rew. B, 73 (2006) 104204.
[19] F. Liu, Q. Yang, S. Pang, C. Ma, T. Zhang, Mater. T., 49 (2008) 231-234.
[20] T. Mizushima, K. Ikarashi, S. Yoshida, A. Makino, A. Inoue, Mat. Trans. JIM, 40 (1999) 1019-1022.
[21] F. Li, T. Zhang, A. Inoue, S. Guan, N. Shen, Intermetallics, 12 (2004) 1139-1142.
[22] M. Xu, M.X. Quan, Z.Q. Hu, L.Z. Cheng, K.Y. He, J. Alloy Compd., 334 (2002) 238-242.
[23] H.W. Chang, Y.C. Huang, C.W. Chang, C.C. Hsieh, W.C. Chang, J. Alloy Compd., 472 (2009) 166-170.
[24] V. Ponnambalam, S.J. Poon, G.J. Shiflet, V.M. Keppens, R. Taylor, G. Petculescu, Appl. Phys. Lett., 83 (2003) 1131-1133.
[25] X.J. Gu, S.J. Poon, G.J. Shiflet, J. Mater. Res., 22 (2007) 344-351.
[26] X.J. Gu, A.G. McDermott, S.J. Poon, G.J. Shiflet, App. Phys. Lett., 88 (2006) 211905.
[27] Z.M. Wang, J. Zhang, X.C. Chang, W.L. Hou, J.Q. Wang, Intermetallics, 16 (2008) 1036-1039.

[28] S.J. Pang, T. Zhang, K. Asami, A. Inoue, Corros. Sci., 44 (2002) 1847-1856.
[29] X.J. Gu, S.J. Poon, G.J. Shiflet, M. Widom, Acta Mater., 56 (2008) 88-94.
[30] J.H. Na, M.D. Demetriou, W.L. Johnson, Appl. Phys. Lett., 99 (2011) 161902.
[31] M. Baricco, A. Castellero, P. Rizzi, G. Riontino, L. Battezzati, Materials Science Forum, 307 (1999) 37.
[32] V.I. Tkatch, S.G. Rassolov, V.V. Popov, S.A. Kostyrya, J. Phys.: Conf. Ser. , 98 (2008) 052011.
[33] Q. Li, Sci. China Ser. E-Technol. Sci., 52 (2009) 1919-1922.
[34] Q. Li, Mater. Lett., 60 (2006) 3113-3117.
[35] K. Russew, S. Bodurov, L. Anestiev, Rapidly Quenched Metals, North Holland, Amsterdam, Netherlands, 1985.
[36] Á. Révész, J. Lendvai, L.K. Varga, I. Bakonyi, Mater. Sci. Forum, 360-362 (2001) 543.
[37] C. Antonione, L. Battezzati, A. Lucci, G. Riontino, G. Venturello, Scripta Metall. Mater., 12 (1978) 1011-1014.
[38] P.M. Anderson, A.E. Lord Jr, J. of Non- Crystalline Solids, 37 (1980) 219.
[39] J. Steinberg, S. Tyagi, A.E. Lord Jr, Acta Metall. , 29 (1981) 1309-1319.
[40] H. Miura, S. Isa, Rapidly Quenched Metals, North Holland, Amsterdam, Netherlands, 1985.
[41] C. Zhang, L. Hu, Y. Yue, J.C. Mauro, J. Chem. Phys. , 133 (2010) 014508.
[42] J.C. Mauro, Y. Yue, A.J. Ellison, P.K. Gupta, D.C. Allan, Proc. Natl. Acad. Sci., 106 (2009) 19780-19784.
[43] I. Gallino, J. Schroers, R. Busch, J. Appl. Phys., 108 (2010) 063501-063501-063501-063508.
[44] I. Gallino, O. Gross, G. Dalla Fontana, Z. Evenson, R. Busch, Journal of Alloys and Compounds 615 (2014) S35–S39.
[45] C.A. Angell, Mrs Bull., 33 (2008) 1-12.

Supporting information

Table A.1 Parameters for different ΔC_p functions, values of T_K and ΔS_g obtained from eq. (15) and m parameters from eqs. (3), (4), (2) using the different functions for ΔC_p for $Fe_{40}Ni_{40}P_{14}B_6$.

Models of ΔC_p	*parameters*	T_K [K]	ΔS_g *[J/mol K]*	m_k from eq. (3)	m_k from eq. (4)	m_k from eq. (2)
$\Delta C_p = A/T$	A = 10617.5	559 ± 24	3.5 ± 0.9	85 ± 38	92 ± 30	92 ± 36
$\Delta C_p = B/T^2$	B = 7272988	537 ± 51	4.9 ± 1.0	71 ± 54	79 ± 57	71 ± 30
$\Delta C_p = C + DT$	C = 20.49594814 D = -0.007293355	587 ± 28	2.5 ± 0.9	111 ± 55	119 ± 73	123 ± 55
$\Delta C_p = ET - FT^2 + GT^{-2}$	E = 0.015745 F= $6.8823*10^{-6}$ G= 3732074	581 ± 32	2.8 ± 0.9	104 ± 73	112 ± 75	111 ± 47

Table A.2 Parameters for different ΔC_p functions, values of T_K and ΔS_g obtained from eq. (15) and m parameters from eqs. (3), (4), (2) using the different functions for ΔC_p of $Fe_{41}Co_7Cr_{15}Mo_{14}C_{15}B_6Y_2$.

Models of ***ΔCp***	*parameters*	T_K *[K]*	ΔS_g [J/mol K]	m_k from eq. (3)	m_k from eq. (4)	m_k from eq. (2)
$\Delta C_p = A/T$	A = 11648	648 ± 17	5.0 ± 0.7	54 ± 10	61 ± 8	61 ± 23
$\Delta C_p = B/T^2$	B = 10436608	652 ± 10	5.8 ± 0.7	55 ± 10	62 ± 7	55 ± 22
$\Delta C_p = C + DT$	C = 27,50871 D = -0,01619	626 ± 14	5.5 ± 1.0	49 ± 8	56 ± 4	57 ± 24
$\Delta C_p = E + F/T$	E = -6,4905 F= 17463,49	644 ± 15	5.5 ± 0.8	53 ± 10	60 ± 6	5 ± 23